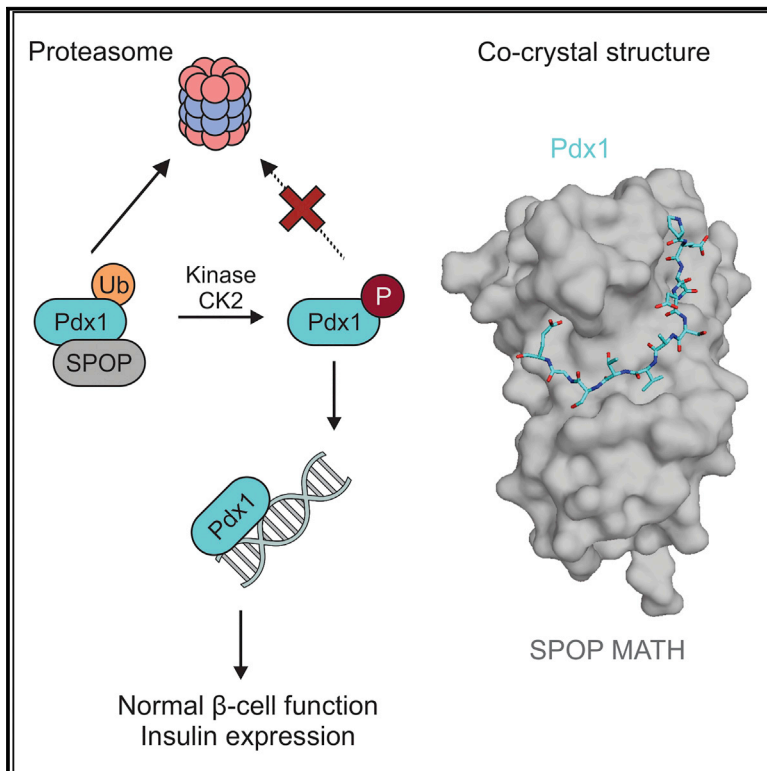


# Structure

## The Structure of the SPOP-Pdx1 Interface Reveals Insights into the Phosphorylation-Dependent Binding Regulation

### Graphical Abstract



### Authors

Michael Sebastian Ostertag,  
Ana Cristina Messias, Michael Sattler,  
Grzegorz Maria Popowicz

### Correspondence

sattler@helmholtz-muenchen.de (M.S.),  
grzegorz.popowicz@  
helmholtz-muenchen.de (G.M.P.)

### In Brief

Ostertag et al. solved the co-crystal structure of SPOP and Pdx1 and studied the effects of Pdx1 phosphorylation on SPOP binding strength. The interaction of the proteins leads to Pdx1 degradation and is considered a key regulatory mechanism for insulin homeostasis.

### Highlights

- SPOP binding to Pdx1 regulates  $\beta$  cell survival and insulin homeostasis
- The co-structure of SPOP/Pdx1 shows features distinct from other SPOP ligands
- Affinity of Pdx1 to SPOP is altered by Pdx1 phosphorylation in the binding site

# The Structure of the SPOP-Pdx1 Interface Reveals Insights into the Phosphorylation-Dependent Binding Regulation

Michael Sebastian Ostertag,<sup>1,2</sup> Ana Cristina Messias,<sup>1,2</sup> Michael Sattler,<sup>1,2,\*</sup> and Grzegorz Maria Popowicz<sup>1,2,3,\*</sup>

<sup>1</sup>Institute of Structural Biology, Helmholtz Zentrum München, Ingolstädter Landstr. 1, Neuherberg 85764, Germany

<sup>2</sup>Center for Integrated Protein Science Munich at Chair of Biomolecular NMR Spectroscopy, Department Chemie, Technische Universität München, Lichtenbergstrasse 4, Garching 85747, Germany

<sup>3</sup>Lead Contact

\*Correspondence: [sattler@helmholtz-muenchen.de](mailto:sattler@helmholtz-muenchen.de) (M.S.), [grzegorz.popowicz@helmholtz-muenchen.de](mailto:grzegorz.popowicz@helmholtz-muenchen.de) (G.M.P.)

<https://doi.org/10.1016/j.str.2018.10.005>

## SUMMARY

Pdx1 is a transcription factor crucial for development and maintenance of a functional pancreas. It regulates insulin expression and glucose homeostasis. SPOP is an E3-ubiquitin ligase adaptor protein that binds Pdx1, thus triggering its ubiquitination and proteasomal degradation. However, the underlying mechanisms are not well understood. Here, we present the crystal structure of the SPOP-Pdx1 complex. We show that Pdx1 residues 223–233 bind to SPOP MATH domain with low micromolar affinity. The interface is extended compared to other SPOP-client proteins. Previously, Pdx1 phosphorylation has been proposed to have a regulatory function. In this respect we show that phosphorylation lowers the affinity of Pdx1 to SPOP by isothermal titration calorimetry and nuclear magnetic resonance data. Our data provide insights into a critical protein-protein interaction that regulates cellular Pdx1 levels by SPOP-mediated decay. A reduction of Pdx1 levels in  $\beta$  cells is linked to apoptosis and considered a hallmark of type 2 diabetes.

## INTRODUCTION

Pdx1 (pancreas/duodenum homeobox protein 1) was identified as a transcription factor responsible for the development of a functional pancreas during embryogenesis (Jonsson et al., 1994). In the adult organism, the protein is responsible for the survival of pancreatic  $\beta$  cells and the regulation of insulin expression and secretion pathways (Ashizawa et al., 2004). Diabetogenic conditions such as glucotoxicity or lipotoxicity were shown to trigger Pdx1 degradation (Robertson, 2004). A decrease of cellular Pdx1 levels leads to apoptosis of the  $\beta$  cells, which is a hallmark of diabetes type 2 (T2D) (Fujimoto and Polonsky, 2009). The degradation of Pdx1 via the ubiquitin-proteasome system is mediated by the E3 ubiquitin ligase adaptor protein SPOP (Speckle-type POZ protein) (Claiborn et al., 2010). SPOP was identified as Pcif1 (Pdx1 C-terminal interacting factor 1)

via co-immunoprecipitation (Liu et al., 2004). SPOP consists of three structured domains. The MATH domain facilitates binding to multiple different client proteins, including Pdx1 (Liu et al., 2006). The BTB/POZ domain, which enables SPOP dimerization, also contains the binding interface to the E3 ubiquitin ligase cullin-3 (Zhuang et al., 2009), which is responsible for substrate ubiquitination (van Geersdaele et al., 2013). The C-terminal domain of SPOP contains an additional dimerization interface, which enables SPOP to form large oligomeric complexes, causing speckle formation in the nucleus. In these speckles, the local SPOP concentration is drastically increased, which presumably increases the ubiquitination turnover of SPOP substrates (Marzahn et al., 2016). Recently it has been shown that SPOP is involved in diverse biological pathways. A mislocalization of SPOP from the nucleus to the cytosol induces tumorigenesis in clear cell renal cell carcinoma (ccRCC) (Li et al., 2014). Mutations in SPOP altering its client protein binding propensities were also found in prostate and endometrial cancer (Dai et al., 2017; Janouskova et al., 2017; Zhang et al., 2017). These findings suggest that SPOP functions as a regulatory hub and that mutations may link SPOP to different diseases.

It was shown that Pdx1 is directly ubiquitinated upon binding to the SPOP-Cullin-3 complex, which leads to its proteasomal degradation (Claiborn et al., 2010). Normal regulatory functions, such as the maintenance of  $\beta$  cell function and the expression of genes such as insulin, islet amyloid peptide (IAPP) and GLUT2, which play key roles in glucose homeostasis, are impaired by the inactivation of Pdx1 (Ashizawa et al., 2004). Declining Pdx1 levels are also linked to  $\beta$  cell death (Fujimoto and Polonsky, 2009). Since SPOP binding triggers Pdx1 degradation, the interaction between SPOP and Pdx1 is considered a key regulatory mechanism for the survival of the pancreatic  $\beta$  cells and ultimately for insulin homeostasis (Figure 1A).

Recently, it was reported that phosphorylation of the Pdx1 SPOP binding site (SBS) has an impact on Pdx1 stability. Specifically, Pdx1 phosphorylation at Thr230 and Ser231 was proposed to increase Pdx1 affinity to SPOP, leading to increased ubiquitination turnover and proteasomal degradation of Pdx1 (Klein et al., 2016). Crystal structures have revealed structural details for the interaction of SPOP with other binding partners, and an SPOP binding consensus (SBC) motif has been proposed (Zhuang et al., 2009). However, the molecular basis for the SPOP-Pdx1 interaction and the potential role of phosphorylation

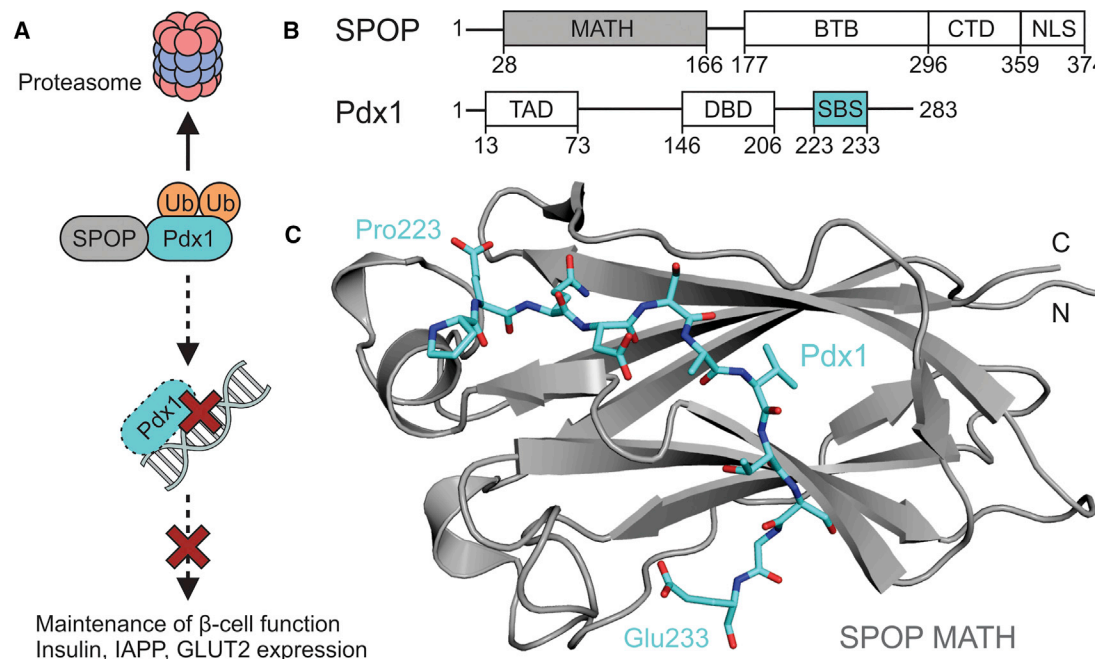


**Figure 1. Structure and Function of the SPOP-Pdx1 Complex**

(A) Cellular pathway of the SPOP-Pdx1 interaction. Upon SPOP binding, Pdx1 is ubiquitinated, which leads to its proteasomal degradation, thus impairing Pdx1 function as a transcription factor. Pdx1-mediated transcriptional regulation of the maintenance of  $\beta$  cell function and the expression of insulin, islet amyloid peptide (IAPP) and GLUT2 genes is thus impaired. Declining Pdx1 levels were linked to  $\beta$  cell death. The SPOP-Pdx1 interaction therefore directly influences  $\beta$  cell survival, insulin expression, and glucose homeostasis.

(B) Schematic display of SPOP and Pdx1 domain organization. SPOP contains a MATH domain (gray) for substrate binding and a BTB domain, which binds the E3-ligase cullin-3 and enables SPOP dimerization. The C-terminal domain (CTD) also contains a dimerization interface. SPOP has a nuclear localization sequence (NLS). Pdx1 contains an N-terminal transactivation domain (TAD) and a DNA binding homeobox domain (DBD). The SPOP binding site (SBS) in Pdx1 is indicated in cyan.

(C) 3D model of SPOP MATH-Pdx1 co-structure. SPOP MATH is shown as gray cartoon. Pdx1 is shown as stick model with carbon atoms shown in cyan, nitrogen atoms in blue, and oxygen atoms in red. SPOP MATH contains a  $\beta$ -sheet core, which interacts with Pdx1 residues 223–233.

were not known. The interaction of SPOP and Pdx1 was initially demonstrated by a yeast two-hybrid screen (Liu et al., 2004). The Pdx1 region required for SPOP binding was mapped to a highly conserved motif in the proximal C-terminus of Pdx1 (Figure 1B) (Liu et al., 2006) via pulldown assays using truncated Pdx1 constructs.

Here, we report a 2 Å resolution crystal structure of the complex of Pdx1 and the SPOP MATH domain (Figure 1C). The structure reveals the specific recognition of Pdx1 by SPOP using features distinct from other SPOP complexes. Using isothermal titration calorimetry (ITC) and nuclear magnetic resonance (NMR) experiments, we studied the binding affinity of the SPOP MATH domain to different regions and to full-length Pdx1. We also show that phosphorylation of the Pdx1 SBS reduces the SPOP interaction in contrast to previous reports. The structural and biophysical data on the SPOP-Pdx1 interface reveal important molecular insights into regulation of cellular Pdx1 levels via the ubiquitin-proteasome-system.

## RESULTS

### Crystal Structure of the SPOP MATH-Pdx1 Complex

We solved co-crystal structures of the human SPOP MATH domain (residues 28–166) with two different Pdx1 peptides

(Table 1). The MATH domain boundaries were chosen according to previously published SPOP structures (Zhuang et al., 2009). Pdx1 peptides are derived from human (residues 222–233) and gold hamster (*Mesocricetus auratus*, residues 223–233) Pdx1. The peptides differ only at position 227 with a Cys in the human sequence and a Ser in the hamster sequence, respectively. The complex structure of hamster Pdx1 and human SPOP MATH contains four individual complexes in the asymmetric unit, while the structure with the human proteins contains a single complex. The overall heavy-atom root-mean-square deviation (RMSD) between all five obtained complexes is below 0.33 Å, indicating nearly identical structures.

An overview of the co-structure and the domain organization of SPOP and Pdx1 is shown in Figure 1C. Pdx1 binds in a long but shallow groove on the SPOP surface. Binding is mediated by extensive hydrogen bonding between the backbones of the two proteins. Several hydrogen bonds (H bonds) between SPOP and Pdx1 are bridged via water molecules (Figure 2). The first water molecule (w1) is bound to Pdx1 via H bonds to Asp226 and Ala228 and is coordinated by SPOP residues Lys134 and Lys135. The second water molecule (w2) is coordinated by Pdx1 Ala228 and Thr230 and bonded to SPOP Lys134. The presence of these water molecules is considered important for SPOP-Pdx1 binding, as they enable the formation

**Table 1. Collection and Refinement Statistics for Crystallographic Data**

|                             | SPOP MATH – Human Pdx1  | SPOP MATH – Hamster Pdx1 |
|-----------------------------|-------------------------|--------------------------|
| Pdx1 fragment sequence      | PEQDCAVTSGE             | EPEQDSA VTSGE            |
| PDB entry code              | 6F8F                    | 6F8G                     |
| Data Collection             |                         |                          |
| Beamline                    | ERSF ID30B              | ERSF ID23-2              |
| Wavelength (Å)              | 0.8266                  | 0.8726                   |
| Space group                 | P6 <sub>5</sub> 2 2     | P1                       |
| Cell dimensions             |                         |                          |
| a, b, c (Å)                 | 53.92, 53.92, 207.41    | 45.40, 55.17, 58.07      |
| α, β, γ (°)                 | 90.000, 90.000, 120.000 | 89.254, 89.888, 86.758   |
| Resolution range (Å)        | 2.00–19.94              | 2.03–100                 |
| Observed reflections        | 118,191                 | 124,076                  |
| Unique reflections          | 13,193                  | 35,062                   |
| Whole range                 |                         |                          |
| Completeness (%)            | 99.0                    | 96.4                     |
| R <sub>meas</sub> (%)       | 3.9                     | 10.6                     |
| I/σ (I)                     | 26.23                   | 8.62                     |
| Last shell                  |                         |                          |
| Resolution (Å)              | 2.00                    | 2.03                     |
| Completeness (%)            | 96.1                    | 80.2                     |
| R <sub>meas</sub> (%)       | 94.3                    | 71.0                     |
| I/σ (I)                     | 1.46                    | 1.79                     |
| Refinement Statistics       |                         |                          |
| No. of reflections          | 12,184                  | 32,906                   |
| Resolution (Å)              | 2.00                    | 2.05                     |
| R factor (%)                | 21.549                  | 18.414                   |
| R <sub>free</sub> (%)       | 27.433                  | 26.169                   |
| Average B (Å <sup>2</sup> ) | 60.815                  | 38.798                   |
| RMSD of bond length (Å)     | 0.017                   | 0.014                    |
| RMSD of angles (°)          | 1.830                   | 1.693                    |
| Content of Asymmetric Unit  |                         |                          |
| No. of protein complexes    | 1                       | 4                        |
| No. of protein atoms        | 1,158                   | 4,802                    |
| No. of solvent atoms        | 35                      | 371                      |

of a network of H bonds. The B factors of these two waters are very similar to the B factors of the main chain atoms from their coordinating SPOP residues Lys134 and Lys135, confirming the accuracy of their position. They are present in all five complexes at equivalent positions.

Additional water-bridged H bonds are formed by C-terminal Pdx1 residues Gly232 (w3) and Glu233 (w4). These waters are not present in all complexes, indicating a non-critical contribution to binding. Pdx1 Glu233 could only be modeled from electron density in two out of five complexes present in the asymmetric units. Here, Pdx1 Glu233 forms an H bond to a water

molecule (w4) buried in a hydrophilic pocket of SPOP. However, in the other complexes, the residue Glu233 was found in a different orientation (away from the SPOP protein) or could not be modeled at all, suggesting a more dynamic character of this interaction.

### Structural Comparison of the SPOP-Pdx1 Co-structure to Other SPOP-Client Structures Reveals Features Required for Pdx1 Binding

We compared our structure (PDB: 6F8G) to published co-structures of SPOP MATH and client proteins, i.e., Puc phosphatase (PDB: 3IVV) and MacroH2A (PDB: 3IVB) (Zhuang et al., 2009) (Figure 3). The heavy-atom RMSDs of SPOP molecules of these three structures are below 0.47 Å, indicating high similarity between the SPOP molecules. There are, however, significant differences in specific ligand recognition.

An SBC motif was previously defined as (φ-p-S-S/T-S/T, φ: nonpolar; p: polar) (Zhuang et al., 2009). Puc and MacroH2A peptides follow this pattern closely with their sequences: Puc<sup>SBC<sub>pep1</sub></sup> (PDB: 3IVV) DEVTSTTSSS, MacroH2A<sup>SBC<sub>pep1</sub></sup> (PDB: 3IVB) KAASADSTTEGTPAD. However, the SBC of hamster Pdx1 has the sequence EPEQDSA VTSGE. Hence, Pdx1 does not follow the SBC motif rigorously, suggesting an extended ligand motif for SPOP clients. A superposition of the structures PDB: 3IVV, PDB: 3IVB and one complex from our structure PDB: 6F8G is shown in Figure 3A.

Pdx1 deviates from the SBC, as it lacks the two Ser/Thr residues (SBC positions 4 and 5) (Figure 3B), having instead a Gly and a Glu residue. This marks an important difference in client binding. A comparison of the interactions formed by the SBC residues of Pdx1 and Puc to SPOP (Figure S1) reveals identical binding modes for Val and Thr (SBC positions 1 and 2) present in both ligands. Pdx1 Val229 is involved in hydrophobic contacts to SPOP, whereas Pdx1 Thr230 forms two H bonds to SPOP residue Gly132. However, the conserved Ser residue (SBC position 3) and its following residues (SBC positions 4 and 5) behave differently in both ligands. In the SPOP-Puc complex, there is a tight network of four H bonds formed by Puc Ser100 and Thr101 to SPOP residue Asp130. The sidechain of Puc Ser100 is involved in up to three alternating H bonds, as shown by the LigPlot analysis (Figure S1), although the geometry of one of these H bonds (to SPOP Asp130 carbonyl) is suboptimal. In the Pdx1 co-structure, two H bonds from Pdx1 Ser231 to SPOP Asp130 are found. Furthermore, SPOP Lys129 forms two H bonds to Puc, but only one H bond to Pdx1. This change in hydrogen bonding is presumably due to the deviation of Pdx1 from the SBC. In the SPOP-Puc co-structure, the sidechain of Thr101 (SBC position 4) is able to form an additional H bond to Asp130, which cannot be formed by Gly232 (SBC position 4) of Pdx1. This additional interaction is assumed to cause a structural change which enables higher H-bond coordination in the Puc interface. This might explain the observed difference in affinity between SPOP MATH and the Puc and Pdx1 peptides. The published dissociation constant ( $K_D$ ) of Puc to SPOP MATH is  $3.7 \pm 0.03 \mu\text{M}$  (determined by surface plasmon resonance [SPR]) (Zhuang et al., 2009), whereas we determined a  $K_D$  of full-length Pdx1 to SPOP MATH as  $65.5 \pm 9.6 \mu\text{M}$  via ITC experiments (Figure S2). While affinities determined with these methods may differ based on the experimental setup, the

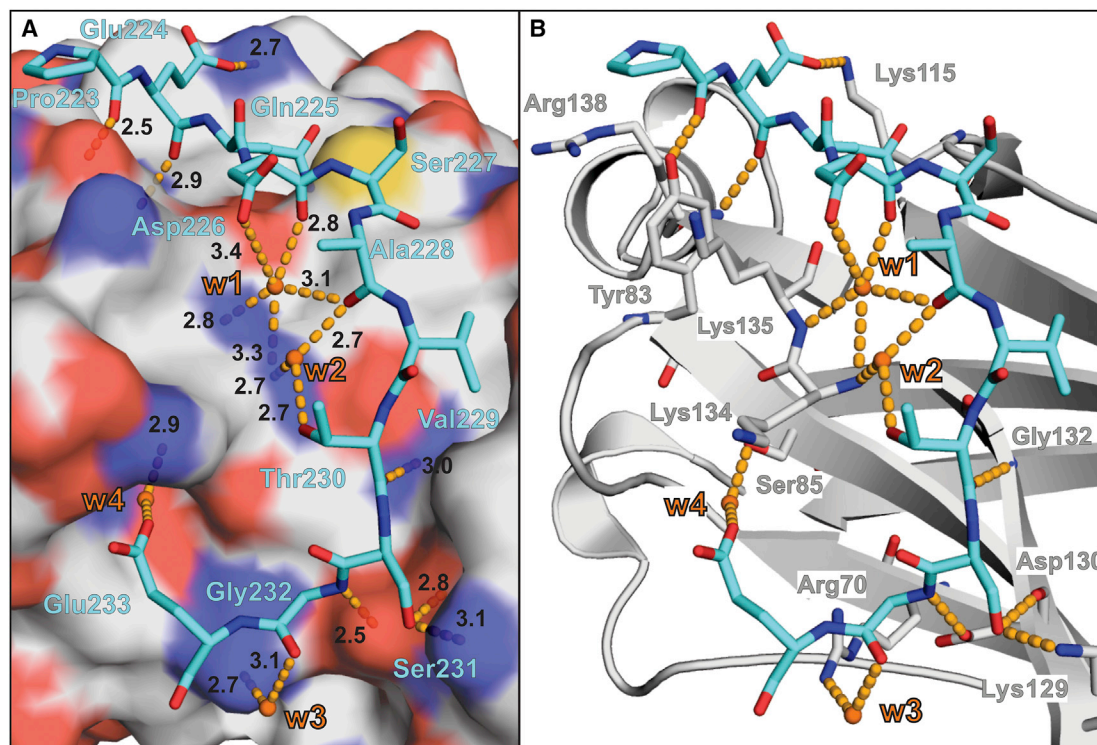


**Figure 2. Detailed View of the Interactions Formed between SPOP and Pdx1**

SPOP carbon atoms are shown in gray. Pdx1 carbon atoms are shown in cyan. Other atoms are colored by type (oxygen = red, nitrogen = blue, sulfur = yellow), water molecules are shown as orange spheres. H bonds are shown as golden dashed lines.

(A) Surface view of SPOP MATH with Pdx1 as stick model. Pdx1 residues are labeled in cyan. Pdx1 residues Asp226, Ala228, Thr230, Gly232, and Glu233 coordinate water molecules, bridging several H bonds to SPOP residues. H bond distances are given in angstroms. (B) SPOP MATH is shown as a gray cartoon. Pdx1 is shown as sticks. SPOP residues involved in the interaction are labeled and shown as sticks. Pdx1 residues are involved in extensive hydrogen bonding to SPOP, including a number of water-mediated hydrogen bonds.

observed difference in affinity by an order of magnitude suggests an altered binding mode.

In contrast to published SPOP-client co-structures, key interacting residues are also found to the N-terminal side of the SBC motif in our SPOP-Pdx1 co-structure (Figure 3A). Here, our Pdx1 fragment contains six additional residues, of which most are involved in binding (Figure 2B). This extended interface and the additional interactions formed are key features determining the specificity of SPOP to Pdx1 and are distinct from other client proteins. It is possible that extended Puc or MacroH2A peptides would be able to form additional contacts to the SPOP protein. However, two N-terminal residues of the MacroH2A could not be modeled from electron density, indicating that these residues do not significantly contribute to SPOP binding.

The analysis of the SPOP MATH-Pdx1 complex demonstrates that the previously proposed SBC motif does not cover all ligands of SPOP and that the SPOP MATH domain can accommodate ligands with sequence variations in the core binding motif and additional contacts with flanking regions.

#### Binding Stoichiometry of SPOP to Full-Length Pdx1 Follows a One-Site Binding Model

Some SPOP clients (e.g., Puc phosphatase) have been shown to contain more than one SBS (Zhuang et al., 2009). We therefore sought to elucidate the stoichiometry of SPOP MATH binding

to Pdx1. Our crystallographic data indicate a 1:1 stoichiometry of SPOP MATH to Pdx1 (residues 222–233). In order to elucidate the stoichiometry of SPOP MATH to the complete Pdx1 protein, we performed ITC experiments titrating SPOP MATH to different Pdx1 constructs (Figure S2). We used Pdx1 DNA binding homeobox domain (DBD)-SBS (146–233) and Pdx1 full-length (1–283), as well as a Pdx1 peptide (219–233) as control. The Pdx1 peptide used for ITC was slightly longer than the peptides (223–233) used for co-crystallization.  $^1\text{H}$ - $^{15}\text{N}$  heteronuclear single quantum coherence (HSQC) NMR experiments with  $^{15}\text{N}$ -labeled Pdx1 DBD-SBS revealed that Pdx1 residue Ala221 shows small chemical shifts upon titration with unlabeled SPOP MATH protein. This indicates that this residue contributes weakly to SPOP binding, and thus the Pdx1 peptide was slightly extended for  $K_D$  determination by ITC.

The ITC data with different Pdx1 constructs confirm the 1:1 stoichiometry seen in the crystal structure also for the interaction of SPOP MATH and full-length Pdx1. The heat changes and the integrated heat plots (Figure S2) show the same binding behavior of SPOP to all three Pdx1 constructs used. When fitted to a one-site binding model, our analysis indicates highly similar  $K_D$ s: SPOP MATH-Pdx1 (219–233):  $K_D = 95.9 \pm 2.0 \mu\text{M}$ , SPOP MATH-Pdx1 (DBD-SBS 146-233):  $K_D = 56.1 \pm 11.3 \mu\text{M}$ , SPOP MATH-Pdx1 (full-length 1–283):  $K_D = 65.5 \pm 9.6 \mu\text{M}$ . These data show that SPOP MATH binds to full-length Pdx1 with a

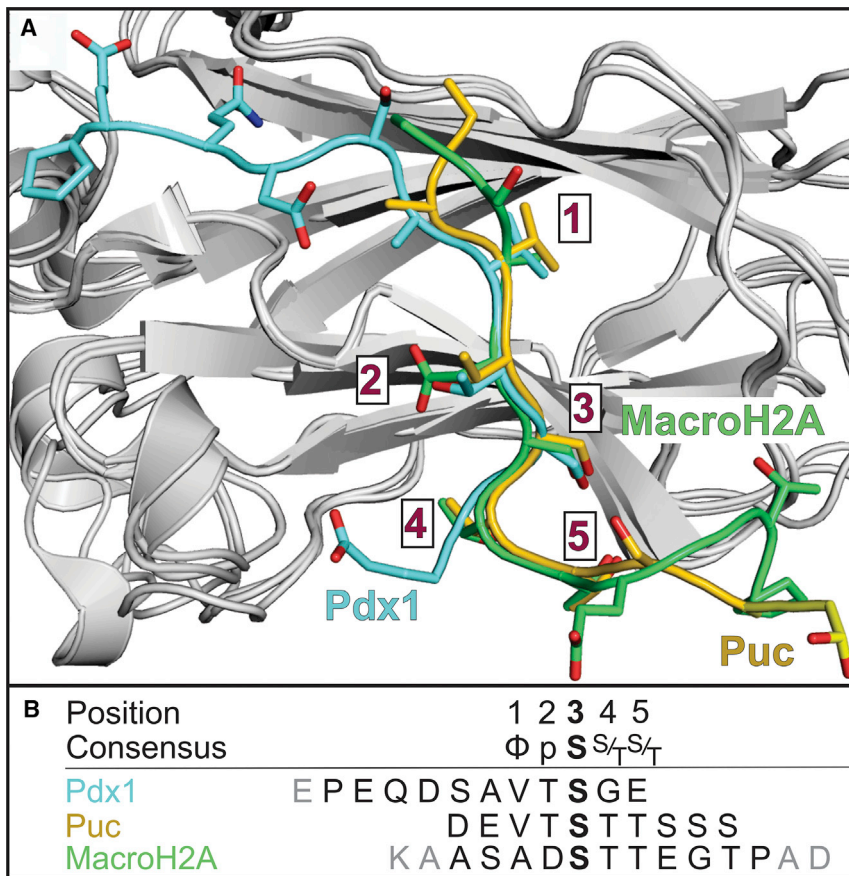


**Figure 3. Comparison of SPOP Co-crystal Structures Containing Different Ligands**

(A) Superimposed display of our SPOP-Pdx1 co-structure (PDB: 6F8G) with SPOP-Puc phosphatase co-structure (PDB: 3IVV) and SPOP-MacroH2A co-structure (PDB: 3IVB). SPOP MATH molecules are displayed as gray cartoons. Ligands are displayed as cartoon with side chains. Pdx1 is shown in cyan, Puc phosphatase in yellow, MacroH2A in green. Numbers indicate SBC positions.

(B) Sequence of Pdx1, Puc, and MacroH2A molecules used for co-crystallization are given. Residues that were not modeled from electron density are shown in gray. The SBC (Zhuang et al., 2009) is shown above ( $\Phi$  = nonpolar, p = polar).

Different SPOP ligands rely on the core binding motif of  $\Phi$ -p-Ser. The orientation of these residues is similar in all interfaces, although Pdx1 is significantly extended to one side compared with Puc and MacroH2. Our data show that SPOP can accommodate ligands such as Pdx1 with amino acid sequences differing from the defined SBC.

95.9  $\mu$ M, phosphorylation of either Ser231 or Thr230 decreases the affinity to 715.8  $\mu$ M and 1.5 mM, respectively. For the doubly phosphorylated Pdx1 peptide, no binding could be detected in ITC experiments.

NMR titrations of SPOP with the different Pdx1 peptides confirm the ITC observations. The overlay of HSQC

1:1 stoichiometry and that a peptide containing residues 219–233 of Pdx1 is sufficient for binding.

To assess if additional contacts are formed between Pdx1 and other SPOP regions, an extended SPOP MATH BTB construct (28–330) was used. Its  $K_D$  to full-length Pdx1 determined via ITC (Figure S2) was  $57.8 \pm 2.1 \mu$ M. This value is identical (within experimental error) to the  $K_D$  of the isolated SPOP MATH domain to full-length Pdx1, thus indicating that no contacts are formed between Pdx1 and the SPOP BTB domain. The MATH domain is therefore considered the only SPOP domain that interacts with Pdx1.

### Phosphorylation of Pdx1 at Thr230 and Ser231 Affects Pdx1 Binding Affinity to SPOP

Thr230 and Ser231 of Pdx1 were previously identified to be phosphorylated by Kinase CK2 (Meng et al., 2010). It was postulated that phosphorylation of Thr230 and Ser231 in Pdx1 affects its stability *in vivo*. The proposed effect of phosphorylation was an increased binding affinity of Pdx1 to SPOP (Klein et al., 2016), which would result in increased ubiquitination and reduced Pdx1 levels. To assess this *in vitro*, we performed ITC experiments, titrating SPOP MATH to peptides of human Pdx1 with different phosphorylation states (Figure S3). The Pdx1 peptides (residues 219–233) were non-phosphorylated, phosphorylated at either Thr230 or Ser231, or phosphorylated at both sites. Surprisingly, we observe a decrease in SPOP binding affinity to phosphorylated Pdx1 peptides compared with non-phosphorylated Pdx1. While the titration of SPOP to non-phosphorylated Pdx1 shows a  $K_D$  of

spectra (Figure 4) shows strong SPOP amide chemical shift perturbations (CSPs) upon titration with non-phosphorylated Pdx1. Weaker CSPs are observed upon titration with Ser231 phosphorylated peptide, which decrease even more when Thr230 phosphorylated peptide is used. These findings correlate well with the binding strengths observed in ITC. The NMR titration of SPOP with doubly phosphorylated Pdx1 (Thr230 and Ser231) shows the weakest CSPs, indicating that this Pdx1 construct binds very weakly to SPOP (Figure S4). However, as opposed to ITC experiments, the very weak binding is still detectable by NMR. In conclusion, ITC and NMR data demonstrate that Pdx1 phosphorylation leads to decreased binding to SPOP.

### The SBS of Pdx1 Is a Structurally Independent Motif from the DNA Binding Domain

The SBS flanks the DBD of Pdx1 (Figure 1B). We therefore wanted to investigate whether intramolecular interactions between the SBS and DBD of Pdx1 could modulate their molecular functions. For this, the Pdx1 construct DBD-SBS (146–233) was used, which contains the DBD (146–206) followed by a glycine-rich linker (207–222) and the SBS (223–233) of Pdx1. The analysis of NMR secondary CSPs (Figure S5A) shows three distinct  $\alpha$ -helical regions in the DBD. These data match well the secondary structure elements in the published crystal structure of the Pdx1 DBD (PDB: 2H1K) (Longo et al., 2007) and confirms that folded Pdx1 is observed. Further, secondary CSP values close

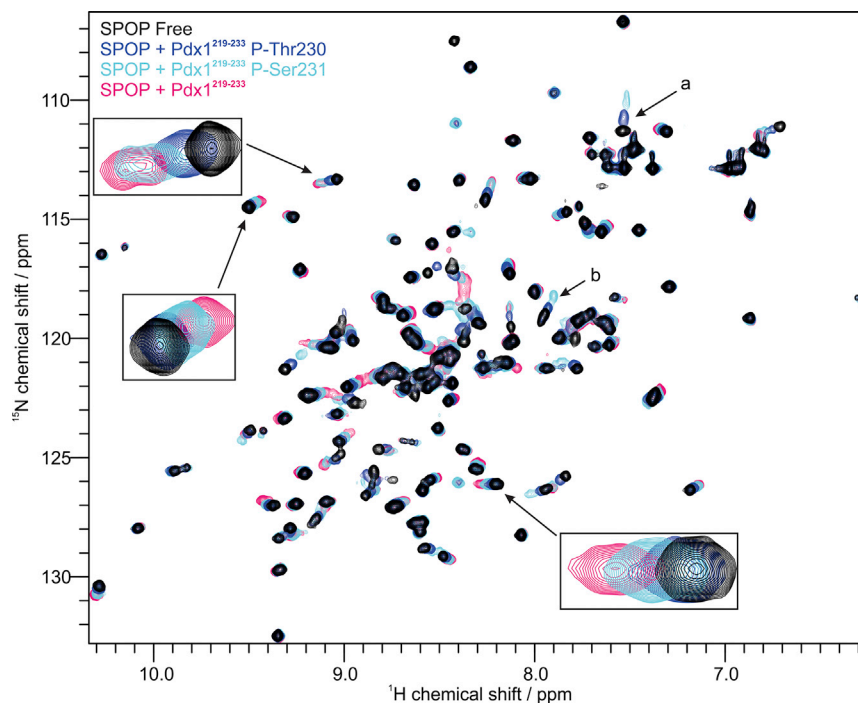


**Figure 4. NMR Titrations of SPOP with Pdx1 in Different Phosphorylation States**

$^{15}\text{N}$ -labeled SPOP MATH (100  $\mu\text{M}$ ) was titrated with 5-fold molar excess of Pdx1 peptides.  $^1\text{H}$ ,  $^{15}\text{N}$  HSQC spectra are shown for SPOP MATH free (black), bound to Pdx1 $^{219-233}$  non-phosphorylated (pink), Pdx1 $^{219-233}$  P-Thr230 (blue), and Pdx1 $^{219-233}$  P-Ser231 (cyan). The CSPs become smaller with increasing Pdx1 phosphorylation. Pdx1 P-Ser231 binds significantly weaker than non-phosphorylated Pdx1, this effect is even more pronounced in Pdx1 P-Thr230. Amide signals of some residues (e.g., peaks a and b) are broadened beyond detection upon titration of SPOP with non-phosphorylated Pdx1, consistent with highest affinity. See Figure S4 for individual spectra overlays.

Pdx1 binding to SPOP. The interaction is mediated by extensive hydrogen bonding as well as a network of H bonds bridged by water molecules. Our structural analysis of the SPOP-Pdx1 interface indicates that SPOP can accommodate ligands with lower amino acid conservation than the previously defined SBC (Zhuang et al., 2009). The interactions with the

to zero show that the linker and the SBS are intrinsically unstructured. This is supported by the  $\{^1\text{H}\}$ - $^{15}\text{N}$  heteronuclear nuclear Overhauser effects (NOEs) of the Pdx1 DBD-SBS construct (Figure S5B), which indicate that the backbone residues of the DBD are rigid while the entire C-terminal region (207–233) is highly dynamic at sub-nanosecond timescales. In particular, the backbone amides of the glycine-rich linker (207–221) and the C-terminus (231–233) are very flexible. Residues 224 to 230 show higher heteronuclear NOE values, suggesting slightly more rigidity in this region. This could indicate that these core residues forming the Pdx1 SBS are already in a slightly extended form for SPOP binding.

We performed NMR titrations of  $^{15}\text{N}$ -labeled Pdx1 DBD-SBS with 5-fold molar excess of unlabeled SPOP MATH (Figure S5C). Analysis of the Pdx1 CSPs upon titration with SPOP reveals that the DBD of Pdx1 remains unaffected by the addition of SPOP. All residues of the SBS (Glu224–Glu233) of Pdx1 are broadened beyond detection in the  $^1\text{H}$ ,  $^{15}\text{N}$  HSQC spectrum upon SPOP addition, possibly reflecting binding kinetics in intermediate exchange at the NMR chemical shift timescale.

Taken together, the NMR data confirm that the DBD and the SBS of Pdx1 are independent motifs. The DBD is unaffected by SPOP binding to the SBS. We therefore conclude that there is no pre-orientation of the SBS by the presence of the DBD. The SBS is intrinsically unstructured but exhibits less flexibility compared with other linker regions, suggesting a partially preformed conformation that may facilitate SPOP binding, possibly due to side chain contacts between neighboring residues.

## DISCUSSION

We present two crystal structures of the SPOP-Pdx1 interaction that reveal critical and unexpected features required for specific

Pdx1 ligand are limited to the SPOP MATH domain, which binds to an 11-residue polypeptide that is significantly extended compared with previously reported structures. Based on our structural analysis and binding data, we propose a more relaxed consensus binding motif for SPOP ligands ( $\phi$ -p-S-p-p,  $\phi$ : nonpolar; p: polar). Notably, a large proportion of the observed H bonds is formed by backbone atoms of the proteins. This rationalizes the relatively broad tolerance of SPOP toward different amino acid sequences, as long as key residues forming important sidechain contacts remain conserved.

We further established that the Pdx1 SBS is a largely unstructured motif that forms an extended conformation in the SPOP bound form. The adjacent DBD neither contributes to the SPOP binding nor modulates the interaction of the SBS.

We also studied the effect of Pdx1 phosphorylation for the SPOP interaction. Pdx1 had been reported to be a target of CK2 kinase, which phosphorylates Pdx1 residues Ser231 and Thr230 (Meng et al., 2010). This phosphorylation was proposed to decrease Pdx1 stability, via an increased affinity to SPOP. This would directly result in increased ubiquitination turnover and proteasomal degradation of Pdx1 (Klein et al., 2016). Surprisingly, our binding data are in contrast to this and do not support this hypothesis. Our NMR and ITC *in vitro* experiments show reduced SPOP binding affinity with increasing phosphorylation of Pdx1 compared with non-phosphorylated Pdx1. The affinities of P-Thr230 and P-Ser231 Pdx1 to SPOP MATH were strongly reduced, while almost no binding was observed for doubly phosphorylated Pdx1.

These data are consistent with the structure of the SPOP-Pdx1 complex. The introduction of one or two phosphate groups to Pdx1 directly in its SBS would cause a significant change in charge and the steric propensities of the ligand. This would impair key contacts that are crucial for binding.

Notably, Thr230 phosphorylation seems more disruptive to binding than Ser231 phosphorylation, presumably because phosphorylation of Thr230 would disrupt the network of water-mediated H bonds critical for binding.

In their experiments, Klein et al. (2016) used phospho-deficient mutants (Thr230Ala, Ser231Ala) and phospho-mimicking mutants (Thr230Asp, Ser231Glu) to study the effects of Pdx1 phosphorylation. Based on our SPOP-Pdx1 co-crystal structure, mutation of Pdx1 residues Thr230 or Ser231 to Ala is expected to significantly reduce the SPOP interaction, as these residues are involved in key H bonds. Mutation of Thr230 to Asp exchanges the hydroxyl group in the sidechain with a carboxyl group. This could potentially enable additional hydrogen bonding at this position, which could strengthen the affinity to SPOP. In fact, some SPOP clients that bind with low micromolar affinity, such as Macro H2A (SPOP co-structure: PDB: 3IVB), have a native Asp residue at this position. Taking this into consideration, the observations by Klein et al. (2016) could have been misinterpreted based on the introduction of the phospho-deficient and phospho-mimicking mutants directly in the Pdx1 SBS and do not represent the effect of actual protein phosphorylation.

It was initially reported that CK2 phosphorylation regulates Pdx1 transcriptional activity (Meng et al., 2010). Pdx1 T230A and S231A single and double-mutants were shown to have elevated transcriptional activity compared with the wild type. Our structural data suggest that in these mutants, SPOP binding would be severely weakened, which could result in reduced ubiquitination and proteasomal degradation of Pdx1, thus increased lifetime and higher transcriptional activity of Pdx1. This suggests the biological significance of Pdx1 phosphorylation at Thr230 and Ser231 as a regulatory mechanism for the SPOP-Pdx1 interaction. The phosphorylation in the Pdx1 SBS motif could function as a regulatory mechanism to maintain cellular Pdx1 levels by inhibiting SPOP binding and subsequent Pdx1 degradation. Such a regulatory mechanism would be beneficial under diabetogenic conditions and at the onset of T2D, as it was shown that preserved Pdx1 expression can improve  $\beta$  cell failure in diabetic mice (Yamamoto et al., 2017).

The SPOP-Pdx1 interaction is assumed to play a key role in  $\beta$  cell survival and thus the maintenance of a functional pancreas. Declining Pdx1 levels were shown to trigger pancreatic  $\beta$  cell death (Fujimoto and Polonsky, 2009). To our knowledge, it is not known whether SPOP is overexpressed in  $\beta$  cells of T2D patients. If so, this would further stress the role of SPOP-mediated Pdx1 decay in the onset of T2D. Thus, the SPOP-Pdx1 interaction could prove to be a valuable target in the effort to develop new antidiabetic therapeutic applications.

## STAR★METHODS

Detailed methods are provided in the online version of this paper and include the following:

- KEY RESOURCES TABLE
- CONTACT FOR REAGENT AND RESOURCE SHARING
- EXPERIMENTAL MODEL AND SUBJECT DETAILS
  - Bacterial Cell Culture

## ● METHOD DETAILS

- Protein Expression and Purification
- Crystallization and X-ray Structure Solution
- NMR Spectroscopy
- Isothermal Titration Calorimetry

## ● DATA AND SOFTWARE AVAILABILITY

- Crystallographic Data
- NMR Backbone Assignment

## SUPPLEMENTAL INFORMATION

Supplemental Information includes five figures and one table and can be found with this article online at <https://doi.org/10.1016/j.str.2018.10.005>.

## ACKNOWLEDGMENTS

We are thankful to Dr. Arie Geerlof (Protein Expression and Purification Facility, HMGU) for providing vectors and proteases required for protein production. We gratefully acknowledge the use of the X-ray Crystallography Platform at the Institute of Structural Biology (HMGU). We thank the European Synchrotron Radiation Facility (Grenoble, France) for beamline access and the Bavarian NMR Center (BNMRZ) for NMR measurement time. M.S. acknowledges support from the DFG Collaborative Research Center, SFB1035.

## AUTHOR CONTRIBUTIONS

M.S.O., G.M.P., and M.S. conceived and designed the experiments. M.S.O. performed the experiments. M.S.O. and G.M.P. recorded and analyzed crystallographic data. M.S.O. and A.C.M. recorded NMR data; M.S.O., A.C.M., and M.S. analyzed NMR data. M.S.O., G.M.P., A.C.M., and M.S. wrote the manuscript.

## DECLARATION OF INTERESTS

The authors declare no competing interests.

Received: May 4, 2018

Revised: August 20, 2018

Accepted: October 10, 2018

Published: November 15, 2018

## REFERENCES

- Ashizawa, S., Brunicardi, F.C., and Wang, X.P. (2004). PDX-1 and the pancreas. *Pancreas* 28, 109–120.
- Bastidas, M., and Showalter, S.A. (2013). Thermodynamic and structural determinants of differential Pdx1 binding to elements from the insulin and IAPP promoters. *J. Mol. Biol.* 425, 3360–3377.
- Claiborn, K.C., Sachdeva, M.M., Cannon, C.E., Groff, D.N., Singer, J.D., and Stoffers, D.A. (2010). Pcf1 modulates Pdx1 protein stability and pancreatic beta cell function and survival in mice. *J. Clin. Invest.* 120, 3713–3721.
- Dai, X., Gan, W., Li, X., Wang, S., Zhang, W., Huang, L., Liu, S., Zhong, Q., Guo, J., Zhang, J., et al. (2017). Prostate cancer-associated SPOP mutations confer resistance to BET inhibitors through stabilization of BRD4. *Nat. Med.* 23, 1063–1071.
- Delaglio, F., Grzesiek, S., Vuister, G.W., Zhu, G., Pfeifer, J., and Bax, A. (1995). NMRPipe: a multidimensional spectral processing system based on UNIX pipes. *J. Biomol. NMR* 6, 277–293.
- Emsley, P., Lohkamp, B., Scott, W.G., and Cowtan, K. (2010). Features and development of Coot. *Acta Crystallogr. D Biol. Crystallogr.* 66 (Pt 4), 486–501.
- Fujimoto, K., and Polonsky, K.S. (2009). Pdx1 and other factors that regulate pancreatic beta-cell survival. *Diabetes Obes. Metab.* 11 (Suppl 4), 30–37.
- Janouskova, H., El Tekle, G., Bellini, E., Udeshi, N.D., Rinaldi, A., Ulbricht, A., Bernasocchi, T., Civenni, G., Losa, M., Svinkina, T., et al. (2017). Opposing effects of cancer-type-specific SPOP mutants on BET protein degradation and sensitivity to BET inhibitors. *Nat. Med.* 23, 1046–1054.

- Jonsson, J., Carlsson, L., Edlund, T., and Edlund, H. (1994). Insulin-promoter-factor 1 is required for pancreas development in mice. *Nature* 371, 606–609.
- Kabsch, W. (2010). Xds. *Acta Crystallogr. D Biol. Crystallogr.* 66 (Pt 2), 125–132.
- Klein, S., Meng, R., Montenarh, M., and Gotz, C. (2016). The phosphorylation of PDX-1 by protein kinase CK2 is crucial for its stability. *Pharmaceuticals (Basel)* 10, <https://doi.org/10.3390/ph10010002>.
- Laskowski, R.A., and Swindells, M.B. (2011). LigPlot+: multiple ligand-protein interaction diagrams for drug discovery. *J. Chem. Inf. Model* 51, 2778–2786.
- Li, G., Ci, W., Karmakar, S., Chen, K., Dhar, R., Fan, Z., Guo, Z., Zhang, J., Ke, Y., Wang, L., et al. (2014). SPOP promotes tumorigenesis by acting as a key regulatory hub in kidney cancer. *Cancer Cell* 25, 455–468.
- Liu, A., Desai, B.M., and Stoffers, D.A. (2004). Identification of PCIF1, a POZ domain protein that inhibits PDX-1 (MODY4) transcriptional activity. *Mol. Cell. Biol.* 24, 4372–4383.
- Liu, A., Oliver-Krasinski, J., and Stoffers, D.A. (2006). Two conserved domains in PCIF1 mediate interaction with pancreatic transcription factor PDX-1. *FEBS Lett.* 580, 6701–6706.
- Longo, A., Guanga, G.P., and Rose, R.B. (2007). Structural basis for induced fit mechanisms in DNA recognition by the Pdx1 homeodomain. *Biochemistry* 46, 2948–2957.
- Marzahn, M.R., Marada, S., Lee, J., Nourse, A., Kenrick, S., Zhao, H., Ben-Nissan, G., Kolaitis, R.M., Peters, J.L., Pounds, S., et al. (2016). Higher-order oligomerization promotes localization of SPOP to liquid nuclear speckles. *EMBO J.* 35, 1254–1275.
- Meng, R., Al-Quobaili, F., Muller, I., Gotz, C., Thiel, G., and Montenarh, M. (2010). CK2 phosphorylation of Pdx-1 regulates its transcription factor activity. *Cell. Mol. Life Sci.* 67, 2481–2489.
- Murshudov, G.N., Vagin, A.A., and Dodson, E.J. (1997). Refinement of macromolecular structures by the maximum-likelihood method. *Acta Crystallogr. D Biol. Crystallogr.* 53 (Pt 3), 240–255.
- Robertson, R.P. (2004). Chronic oxidative stress as a central mechanism for glucose toxicity in pancreatic islet beta cells in diabetes. *J. Biol. Chem.* 279, 42351–42354.
- Studier, F.W. (2005). Protein production by auto-induction in high density shaking cultures. *Protein Expr. Purif.* 41, 207–234.
- Vagin, A., and Teplyakov, A. (2010). Molecular replacement with MOLREP. *Acta Crystallogr. D Biol. Crystallogr.* 66 (Pt 1), 22–25.
- van Geersdaele, L.K., Stead, M.A., Harrison, C.M., Carr, S.B., Close, H.J., Rosbrook, G.O., Connell, S.D., and Wright, S.C. (2013). Structural basis of high-order oligomerization of the cullin-3 adaptor SPOP. *Acta Crystallogr. D Biol. Crystallogr.* 69 (Pt 9), 1677–1684.
- Vranken, W.F., Boucher, W., Stevens, T.J., Fogh, R.H., Pajon, A., Llinas, M., Ulrich, E.L., Markley, J.L., Ionides, J., and Laue, E.D. (2005). The CCPN data model for NMR spectroscopy: development of a software pipeline. *Proteins* 59, 687–696.
- Winn, M.D., Ballard, C.C., Cowtan, K.D., Dodson, E.J., Emsley, P., Evans, P.R., Keegan, R.M., Krissinel, E.B., Leslie, A.G., McCoy, A., et al. (2011). Overview of the CCP4 suite and current developments. *Acta Crystallogr. D Biol. Crystallogr.* 67 (Pt 4), 235–242.
- Wishart, D.S., and Sykes, B.D. (1994). The <sup>13</sup>C chemical-shift index: a simple method for the identification of protein secondary structure using <sup>13</sup>C chemical-shift data. *J. Biomol. NMR* 4, 171–180.
- Yamamoto, Y., Miyatsuka, T., Sasaki, S., Miyashita, K., Kubo, F., Shimo, N., Takebe, S., Watada, H., Kaneto, H., Matsuoka, T.A., and Shimomura, I. (2017). Preserving expression of Pdx1 improves beta-cell failure in diabetic mice. *Biochem. Biophys. Res. Commun.* 483, 418–424.
- Zhang, P., Wang, D., Zhao, Y., Ren, S., Gao, K., Ye, Z., Wang, S., Pan, C.W., Zhu, Y., Yan, Y., et al. (2017). Intrinsic BET inhibitor resistance in SPOP-mutated prostate cancer is mediated by BET protein stabilization and AKT-mTORC1 activation. *Nat. Med.* 23, 1055–1062.
- Zhuang, M., Calabrese, M.F., Liu, J., Waddell, M.B., Nourse, A., Hammel, M., Miller, D.J., Walden, H., Duda, D.M., Seyedin, S.N., et al. (2009). Structures of SPOP-substrate complexes: insights into molecular architectures of BTB-Cul3 ubiquitin ligases. *Mol. Cell* 36, 39–50.

## STAR★METHODS

### KEY RESOURCES TABLE

| REAGENT or RESOURCE   | SOURCE   | IDENTIFIER  |
|---|--|---|
| <b>Bacterial and Virus Strains</b>  |  |   |
| E. Coli Rosetta2 DE3  | own production   | N/A   |
| E. Coli BL21 DE3  | own production   | N/A   |
| <b>Chemicals, Peptides, and Recombinant Proteins</b>  |  |   |
| Human Pdx1 peptide for crystallization (222-233)  | Peptide Specialty Laboratories GmbH, Heidelberg, Germany | ID.Nr.: 68-15-15  |
| Hamster Pdx1 peptide for crystallization (223-233)  | Peptide Specialty Laboratories GmbH, Heidelberg, Germany | ID.Nr.: 30-05-15  |
| Human Pdx1 peptide non-phosphorylated (219-233)   | Peptide Specialty Laboratories GmbH, Heidelberg, Germany | ID.Nr.: 35-10-17  |
| Human Pdx1 peptide Ser231 phosphorylated (219-233)  | Peptide Specialty Laboratories GmbH, Heidelberg, Germany | ID.Nr.: 33-03-17  |
| Human Pdx1 peptide Thr230 phosphorylated (219-233)  | Peptide Specialty Laboratories GmbH, Heidelberg, Germany | ID.Nr.: 33-02-17  |
| Human Pdx1 peptide Thr230 and Ser231 phosphorylated (219-233)                               | Peptide Specialty Laboratories GmbH, Heidelberg, Germany | ID.Nr.: 33-04-17  |
| <b>Deposited Data</b>   |  |   |
| Co-crystal structure of SPOP MATH-PucSBC1_pep1  | <a href="#">Zhuang et al., 2009</a>                      | PDB: 3IVV   |
| Co-crystal structure of SPOP MATH-MacroH2ASBC_pep1  | <a href="#">Zhuang et al., 2009</a>                      | PDB: 3IVB   |
| NMR Backbone assignment of Pdx1 fragment  | <a href="#">Bastidas and Showalter, 2013</a>             | BMRB: 19227   |
| Co-crystal structure of SPOP MATH and human Pdx1 fragment                                   | this study   | PDB: 6F8F   |
| Co-crystal structure of SPOP MATH and hamster Pdx1 fragment                                 | this study   | PDB: 6F8G   |
| Backbone <sup>1</sup> H, <sup>15</sup> N chemical shift assignments of human Pdx1 (146-233) | this study   | BMRB: 27582   |
| <b>Recombinant DNA</b>  |  |   |
| Recombinant DNA of SPOP MATH (28-166)   | IDT Germany GmbH, Munich, Germany                        | N/A   |
| Recombinant DNA of SPOP MATH BTB (28-330)   | IDT Germany GmbH, Munich, Germany                        | N/A   |
| Recombinant DNA of Pdx1 DBD-SBS (146-233)   | IDT Germany GmbH, Munich, Germany                        | N/A   |
| Recombinant DNA of Pdx1 full-length (1-283)   | IDT Germany GmbH, Munich, Germany                        | N/A   |
| <b>Software and Algorithms</b>  |  |   |
| XDS / XSCALE  | <a href="#">Kabsch, 2010</a>                             | <a href="http://xds.mpimf-heidelberg.mpg.de/">http://xds.mpimf-heidelberg.mpg.de/</a>   |
| Molrep v.11.0   | <a href="#">Vagin and Teplyakov, 2010</a>                | <a href="http://www.ccp4.ac.uk/html/molrep.html">http://www.ccp4.ac.uk/html/molrep.html</a>   |
| Coot v.0.8.8  | <a href="#">Emsley et al., 2010</a>                      | <a href="https://www2.mrc-lmb.cam.ac.uk/personal/pemsley/cool/">https://www2.mrc-lmb.cam.ac.uk/personal/pemsley/cool/</a>                                     |
| Refmac5   | <a href="#">Murshudov et al., 1997</a>                   | <a href="http://www.ccp4.ac.uk/html/refmac5.html">http://www.ccp4.ac.uk/html/refmac5.html</a>   |
| CCP4 suite v.7.0  | <a href="#">Winn et al., 2011</a>                        | <a href="http://www.ccp4.ac.uk/index.php">http://www.ccp4.ac.uk/index.php</a>   |
| PyMol Molecular Graphics System v.1.8.6.0   | Schrödinger, LLC   | <a href="https://pymol.org/2/">https://pymol.org/2/</a>   |
| LigPlot+ v.1.4  | <a href="#">Laskowski and Swindells, 2011</a>            | <a href="https://www.ebi.ac.uk/thornton-srv/software/LigPlus/download.html">https://www.ebi.ac.uk/thornton-srv/software/LigPlus/download.html</a>             |
| Topspin v.3.2   | Bruker BioSpin   | <a href="https://www.bruker.com/service/support-upgrades/software-downloads/nmr/">https://www.bruker.com/service/support-upgrades/software-downloads/nmr/</a> |
| NMRPipe v.8.9   | <a href="#">Delaglio et al., 1995</a>                    | <a href="https://www.ibbr.umd.edu/nmrpipe/install.html">https://www.ibbr.umd.edu/nmrpipe/install.html</a>   |

(Continued on next page)

### Continued

| REAGENT or RESOURCE                     | SOURCE                | IDENTIFIER  |
|---|-----------------------|---|
| CCPN Analysis v.2.4.1                   | Vranken et al., 2005  | <a href="https://www.ccpn.ac.uk/v2-software/downloads">https://www.ccpn.ac.uk/v2-software/downloads</a>   |
| MicroCal PEAQ-ITC Analysis v.1.0.0.1259 | Malvern Pananalytical | <a href="https://www.malvernpanalytical.com/de/support/product-support/microcal-range/microcal-itc-range/microcal-peaq-itc-range/microcal-peaq-itc/index.html">https://www.malvernpanalytical.com/de/support/product-support/microcal-range/microcal-itc-range/microcal-peaq-itc-range/microcal-peaq-itc/index.html</a> |

### CONTACT FOR REAGENT AND RESOURCE SHARING

Further information and requests for resources and reagents should be directed to and will be fulfilled by the Lead Contact, Dr. Grzegorz Popowicz ([Grzegorz.popowicz@helmholtz-muenchen.de](mailto:Grzegorz.popowicz@helmholtz-muenchen.de))

### EXPERIMENTAL MODEL AND SUBJECT DETAILS

#### Bacterial Cell Culture

Bacterial strain *E. coli* BL21 DE3 was used for recombinant expression of SPOP proteins (SPOP MATH and SPOP MATH BTB) in vector pETM-11. The strain *E. coli* Rosetta2 DE3 was used for recombinant expression of Pdx1 proteins (Pdx1 DBD-SBS and Pdx1 full-length) in vector pETHSu. Vectors were kindly provided by Dr. Arie Geerlof (STB, HMGU). Pre-cultures were grown in LB medium for approx. 18h at 37°C, 220 rpm. They were used to inoculate expression cultures (1:100) which were then grown at 37°C, 220 rpm until they reached an optical density (600 nm) of approx. 1.0. Cultures were then transferred to 20°C, 220 rpm and incubated further for at least 20 h. The media used for expression cultures were either ZYM-5052 auto-induction medium (Studier, 2005) for unlabeled protein, <sup>15</sup>N-5052 auto-induction medium (Studier, 2005) for uniform labeling with <sup>15</sup>N or M9-based minimal medium containing <sup>13</sup>C-glucose and <sup>15</sup>N-ammonium chloride for uniform labeling with <sup>13</sup>C, <sup>15</sup>N for NMR applications.

### METHOD DETAILS

#### Protein Expression and Purification

Human SPOP MATH (residues 28-166) or SPOP MATH BTB (28-330) were cloned into the pETM-11 vector and expressed in *E. coli* as described above. Two Pdx1 constructs were designed, Pdx1 full-length (1-283) and Pdx1 DBD-SBS (146-233), which contains the DNA binding domain and the SPOP binding site. Pdx1 constructs were cloned into pETHSu vector and expressed in *E. coli* Rosetta2 DE3 cells as described above. Shorter Pdx1 fragments were purchased from Peptide Specialty Laboratories GmbH (Heidelberg, Germany). After cultivation, bacterial cultures were transferred to a buffer containing 100 mM Tris pH 8.0, 300 mM NaCl, 20 mM imidazole, 5 mM β-mercaptoethanol (β-ME) and lysed using a Bandelin Sonopuls HD2070 ultrasonic homogenizer. SPOP proteins were purified from clarified cell lysate via IMAC using a Ni-NTA column. Clarified lysates containing Pdx1 proteins were first subjected to DNA precipitation by adding 0.5% (v/v) polyethyleneimine (PEI), then to ammonium sulfate precipitation before the IMAC step. After IMAC elution with a buffer containing 100 mM Tris pH 8.0, 300 mM NaCl, 300 mM imidazole, 5 mM β-ME, SPOP proteins were dialyzed to TEV cleavage buffer (100 mM Tris-HCl pH 8.0, 100 mM NaCl, 5 mM β-ME) over night at 4°C. TEV protease was subsequently added (1:50) and further incubated overnight at 4°C. To Pdx1 proteins, the SUMO-hydrolase dtUD1 (1:50) was added directly after IMAC elution and incubated overnight at 4°C. After cleavage, all proteins were subjected to a second (reverse) Ni-NTA affinity chromatography step. Proteins were further purified via SEC using a HiLoad 16/60 Superdex 75 preparative grade (pg) column (SPOP MATH, Pdx1 DBD-SBS) or a HiLoad 16/600 Superdex 200 pg column (SPOP MATH BTB, full-length Pdx1) (Äkta system, GE Healthcare). The buffers used for SEC were PBS (137 mM NaCl, 2.7 mM KCl, 10 mM Na<sub>2</sub>HPO<sub>4</sub>, 1.8 mM KH<sub>2</sub>PO<sub>4</sub> pH 7.4, 5 mM β-ME) for NMR, ITC or crystallization buffer (5 mM Tris-HCl pH 8.0, 50 mM NaCl, 5 mM β-ME).

#### Crystallization and X-ray Structure Solution

SPOP MATH was mixed with five-fold molar excess of human Pdx1 peptide (PEQDCAVTSGE, *Homo sapiens* Pdx1 residues 223-233) or hamster Pdx1 peptide (EPEQDSAVTSGE, *Mesocricetus auratus* Pdx1 residues 222-233). The mix was concentrated to 33 mg/ml. The complex of SPOP MATH and human Pdx1 peptide crystallized in 0.1 M HEPES pH 6.5, 10% (w/v) PEG6000 (final pH 7.0) within two weeks at 4°C. The complex of SPOP MATH and hamster Pdx1 peptide crystallized in 0.1 M Imidazole-HCl pH 8.0, 30% (w/v) MPD, 10% (w/v) PEG-4000 within 1 week at room-temperature. The crystals were measured at the ID30b and ID23-2 beamlines of the ESRF, Grenoble, France and yielded datasets of atomic resolution. The obtained datasets were processed using the XDS and XSCALE software (Kabsch, 2010). The structure PDB: 3IVV was used as search model for molecular replacement using Molrep v.11.0 (Vagin and Teplyakov, 2010). Models were rebuilt using Coot v.0.8.8 (Emsley et al., 2010) and iteratively refined using Refmac5 (Murshudov et al., 1997) from the CCP4 suite v.7.0 (Winn et al., 2011). Data collection and refinement statistics are given in Table 1.

Structure figures and RMSD calculations were generated using the PyMol Molecular Graphics System v.1.8.6.0, Schrödinger, LLC. Interaction diagrams were created using the program LigPlot+ v.1.4 (Laskowski and Swindells, 2011).

### NMR Spectroscopy

All NMR spectra were recorded on a Bruker Avance 600 spectrometer with QCI cryogenic probe at 298K using Topspin v.3.2 (Bruker BioSpin). Spectra were processed using NMRPipe v.8.9 (Delaglio et al., 1995) and analyzed using CCPN Analysis v.2.4.1 (Vranken et al., 2005).

Backbone chemical shift assignments for Pdx1 DBD-SBS were obtained from HNCACB and CBCACONH spectra, as well as a published assignment of the Pdx1 DBD (BMRB: 19227) (Bastidas and Showalter, 2013) for reference. They are deposited in the BMRB database as BMRB: 27582. Spectra were acquired using 300  $\mu\text{M}$   $^{13}\text{C}$ ,  $^{15}\text{N}$ -labeled Pdx1 DBD-SBS in PBS pH 7.4, 10%  $\text{D}_2\text{O}$ , 5 mM  $\beta$ -ME. HNCACB acquisition times were 141.9 ms ( $^1\text{H}$ ), 14.1 ms ( $^{15}\text{N}$ ) and 4.9 ms ( $^{13}\text{C}$ ) with a total experimental duration of 2 d 2.5 h. CBCACONH acquisition times were 141.9 ms ( $^1\text{H}$ ), 16.4 ms ( $^{15}\text{N}$ ) and 4.8 ms ( $^{13}\text{C}$ ) with a total experimental duration of 1 d 10.3 h.  $^{13}\text{C}$  secondary chemical shift perturbation values for secondary structure analysis were calculated from  $C\alpha/C\beta$  shifts obtained from the HNCACB spectrum according to the formula  $[(\delta^{13}\text{C}\alpha(\text{observed}) - \delta^{13}\text{C}\alpha(\text{random coil})) - (\delta^{13}\text{C}\beta(\text{observed}) - \delta^{13}\text{C}\beta(\text{random coil}))]$  (Wishart and Sykes, 1994).  $\{^1\text{H}\}$ - $^{15}\text{N}$  heteronuclear NOEs of Pdx1 DBD-SBS were measured using 300  $\mu\text{M}$   $^{13}\text{C}$ ,  $^{15}\text{N}$ -labeled Pdx1 DBD-SBS in PBS pH 7.4, 10%  $\text{D}_2\text{O}$ , 5 mM  $\beta$ -ME, with acquisition times of 141.9 ms ( $^1\text{H}$ ), 140.3 ms ( $^{15}\text{N}$ ) and a total duration of 20.3 h. The signal intensity ratio (NOE/noNOE), and the error propagation based on spectrum noise was obtained using the hetNOE tool of *CCPN Analysis*. Duplicate experiments were measured. NMR titrations were performed by recording  $^1\text{H}$ ,  $^{15}\text{N}$  HSQC experiments. For titrations of Pdx1 DBD-SBS, samples of 100  $\mu\text{M}$   $^{15}\text{N}$ -labeled Pdx1 DBD-SBS in PBS pH 7.4, 10%  $\text{D}_2\text{O}$ , 5 mM  $\beta$ -ME were used. Samples contained either no ligand (reference), or five-fold excess of unlabeled SPOP MATH. Spectra were recorded using acquisition times of 106.5 ms ( $^1\text{H}$ ), 120.3 ms ( $^{15}\text{N}$ ) with a total duration of 4.3 h. For titrations of SPOP MATH with Pdx1,  $^1\text{H}$ ,  $^{15}\text{N}$  HSQC experiments were recorded using samples containing 100  $\mu\text{M}$   $^{15}\text{N}$ -labeled SPOP MATH in PBS pH 7.4, 10%  $\text{D}_2\text{O}$ , 5 mM  $\beta$ -ME. Samples contained either no ligand (reference) or five-fold molar excess of Pdx1<sup>219-233</sup>, either in non-phosphorylated, mono-phosphorylated (P-Thr230, P-Ser231) or doubly-phosphorylated (P-Thr230 & P-Ser231) variants. Spectra were recorded with acquisition times of 106.4 ms ( $^1\text{H}$ ), 60.1 ms ( $^{15}\text{N}$ ) for a total duration of 1.3 h.

### Isothermal Titration Calorimetry

All titrations were performed using the MicroCal PEAQ-ITC (Malvern) at 25.1°C. All used proteins were dialyzed to identical PBS pH 7.4 buffer for at least 18h. Measurements were done with titrant concentrations between 2 mM and 4 mM. Cell sample concentrations varied between 100  $\mu\text{M}$  and 200  $\mu\text{M}$ . The runs consisted of 19 injections with a volume of 2  $\mu\text{L}$  and a duration of 4 seconds each. The first injection with a volume of 0.4  $\mu\text{L}$  and a duration of 0.8 seconds was discarded in the evaluation. The syringe stirring speed was 750 rpm for all runs. The spacing for different runs varied between 120 or 150 seconds. Raw data were processed and integrated using the MicroCal PEAQ-ITC Analysis Software v.1.0.0.1259 (Malvern). During analysis, a control run of syringe titrant to buffer was deducted to exclude heat of dilution. The resulting values in  $\Delta\text{H}/\text{mol}$  were plotted over the molar ratio. The data points were fitted using an appropriate binding model. For SPOP titrations to Pdx1 constructs, a one-site binding model was assumed based on crystallographic data and curve shape. All measurements were performed in triplicate. Detailed results are listed in Table S1. The values given are averages of the triplicates, with the standard deviation given as error.

## DATA AND SOFTWARE AVAILABILITY

### Crystallographic Data

The accession number for the co-crystal structure of SPOP MATH and human Pdx1 reported in this paper is PDB: 6F8F. The accession number for the co-crystal structure of SPOP MATH and hamster Pdx1 reported in this paper is PDB: 6F8G.

### NMR Backbone Assignment

The accession number for the NMR backbone assignment of Pdx1 DBD-SBS (146-233) reported in this paper is BMRB: 27582.